

Fig. 5. Arrhenius plot of the cyclization of **1-PdCl₂** to **4a**. Each point is an average of two or more runs.

30,000 times over the unpromoted reaction (24). The activation parameters for this process ($[1\text{-PdCl}_2] = 0.025\text{ M}$, $[\text{CHD}] = 0.5\text{ M}$, temperature $T = 278\text{ to }308\text{ K}$) are activation energy $E_a = 12.3\text{ kcal mol}^{-1}$ and $\ln(A) = 13.9$ (Fig. 5), reflecting the ease of cyclization under these conditions (25).

We have developed an enediyne-based diphosphine which upon coordination of **1** to palladium or platinum dichloride undergoes a Bergman cyclization at an enormously enhanced rate. In contrast, complexation of **1** to mercuric chloride prevents this cyclization. This system meets the criteria of speed, compatibility, stability, and ease of synthesis presented above. Under appropriate conditions, including in the presence of palladium or platinum dichloride, **1** undergoes rapid cyclization at low temperatures.

REFERENCES AND NOTES

- R. Jones and R. G. Bergman, *J. Am. Chem. Soc.* **94**, 660 (1972).
- K. C. Nicolaou, G. Zuccarello, Y. Ogawa, E. J. Schweiger, T. Kumazawa, *ibid.* **110**, 4866 (1988); K. C. Nicolaou and W.-M. Dai, *Angew. Chem. Int. Ed. Engl.* **30**, 1387 (1991).
- M. D. Lee, *J. Am. Chem. Soc.* **109**, 3464 (1987); J. Golik *et al.*, *ibid.*, p. 3462.
- M. F. Semmelhack *et al.*, *J. Org. Chem.* **59**, 4357 (1994).
- K. C. Nicolaou *et al.*, *Angew. Chem. Int. Ed. Engl.* **30**, 1032 (1991).
- K. C. Nicolaou, W.-M. Dai, S.-C. Tsay, V. A. Estevez, W. Wrasidlo, *Science* **256**, 1172 (1992).
- D. L. Boger and J. Zhou, *J. Org. Chem.* **58**, 3018 (1993).
- K. C. Nicolaou, A. L. Smith, E. W. Yue, *Proc. Natl. Acad. Sci. U.S.A.* **90**, 5881 (1993).
- J. M. Nuss and M. M. Murphy, *Tetrahedron Lett.* **35**, 37 (1994).
- B. König and H. Rütters, *ibid.*, p. 3501.
- P. J. Loehrer and L. H. Einhorn, *Ann. Intern. Med.* **100**, 704 (1984).
- 1,2-Bis(trimethylsilyl)ethynylbenzene [S. Takahashi, Y. Kuroyama, K. Sonogashira and N. Hagihara, *Synthesis* **1980**, 627 (1980)] was converted to **1** by desilylative phosphorylation with potassium *tert*-butoxide in the presence of diphenylphosphoryl chloride. Characterization of **1**: Isolated yield 88%. ¹H NMR (250 MHz, C₆D₆): δ 6.67 (dd, coupling constant, $J = 3.4\text{ Hz}$, 5.8 Hz, 2 H), 6.98 to 7.08 (m, 12 H), 7.19 (dd, $J = 3.4\text{ Hz}$, 5.8 Hz, 2 H), and 7.78 (dd, $J = 6.9\text{ Hz}$, 8.2 Hz, 8 H). ¹³C NMR (75 MHz, CDCl₃): δ 136.94 (d, $J_{\text{CP}} = 6.1\text{ Hz}$), 135.92, 132.69, 132.41, 128.87, 128.63, 128.53, 125.23, 105.96, and 90.54 (d, $J_{\text{CP}} = 9\text{ Hz}$). ³¹P NMR (121 MHz, C₆D₆): δ -32.0. Infrared (IR, film):

- 3285, 3053, 3002, 2954, 2278, 2161, 1954, 1890, 1811, 1752, 1585, 1477, 1434, 1327, 1305, 1274, 1247, 1230, 1204, 1182, 1158, 1097, 1068, 1026, 999, 951, 912, 873, 842, 809, 739, 695, 642, and 632 cm⁻¹. Analysis: calculated for C₃₄H₂₄P₂: C, 82.58%; H, 4.89%; found: C, 82.48%; H, 5.09%.
- N. L. Allinger, *J. Am. Chem. Soc.* **99**, 8127 (1977). Calculated on a Tektronix CAChe worksystem (version 2, 1990), with augmented force fields for atoms not parameterized in MM2.
- Compound **1** was found to bind to Pd(II)Cl₂, Pt(II)Cl₂, and Hg(II)Cl₂, as determined by ¹H NMR.
- R. H. Grubbs and D. Kratz, *Chem. Ber.* **126**, 149 (1993).
- J. A. John and J. M. Tour, *J. Am. Chem. Soc.* **116**, 5011 (1994).
- Heating rate of 20°C min⁻¹ on a Perkin-Elmer DSC 7 differential scanning calorimeter.
- T. P. Lockhart, P. B. Comita, R. G. Bergman, *J. Am. Chem. Soc.* **103**, 4082 (1981).
- Characterization of **4a**: Isolated yield, 92%. Melting point (324°C (decomposes)). ¹H NMR (300 MHz, CD₂Cl₂): δ 7.46 (t, $J = 6.7\text{ Hz}$, 8 H), 7.54 (d, $J = 7.5\text{ Hz}$, 4 H), 7.66 (dd, $J = 3.2\text{ Hz}$, 6.2 Hz, 2 H), 7.78 (dd, $J = 7.5\text{ Hz}$, 12.4 Hz, 8 H), 7.89 (dd, $J = 3.2\text{ Hz}$, 6.2 Hz, 2 H), and 8.08 (d, $J = 11\text{ Hz}$, 2 H). ¹³C NMR (75 MHz, CD₂Cl₂): δ 134.43, 134.37, 134.30, 132.35, 130.06, 129.34, 129.24, 129.18, and 129.11. ³¹P NMR (121 MHz, CD₂Cl₂): δ 62.05. Analysis: calculated for C₃₄H₂₆Cl₂P₂Pd: C, 60.60%; H, 3.89%; found: C, 60.64%; H, 3.99%. Characterization of **4b**: Isolated yield, 75%. Melting point >400°C (decomposes). ¹H NMR (300 MHz, CD₂Cl₂): δ 7.42 to 7.50 (m, 8 H), 7.50 to 7.55 (m, 4 H), 7.66 (dd, $J = 3.2\text{ Hz}$, 6.2 Hz, 2 H), 7.75 to 7.82 (m, 8 H), 7.89 (dd, $J = 3.4\text{ Hz}$, 6.4 Hz, 2 H), and

- 8.11 (d, $J = 12.2\text{ Hz}$, 2 H). ¹³C NMR (75 MHz, CD₂Cl₂): δ 134.54, 134.47, 134.39, 132.45, 130.20, 129.52, 129.42, 129.34, and 129.27. ³¹P NMR (121 MHz, CD₂Cl₂): δ 39.6 (d, $J_{\text{P-Pt}} = 3596\text{ Hz}$). Analysis: calculated for C₃₄H₂₆Cl₂P₂Pt: C, 53.56%; H, 3.44%; found: C, 53.85%; H, 3.62%.
- A. Pryde, B. L. Shaw, B. Weeks, *J. Chem. Soc. Dalton Trans.* **1976**, 322 (1976); F. S. M. Hassan, D. P. Markham, P. G. Pringle, B. L. Shaw, *ibid.* **1985**, 279 (1985).
- Atta-Ur-Rahman, *Nuclear Magnetic Resonance: Basis Principles* (Springer-Verlag, New York, 1986), pp. 131–133.
- D. K. Lewis *et al.*, *J. Am. Chem. Soc.* **115**, 11728 (1993).
- M. F. Semmelhack, T. Neu, F. Foubelo, *Tetrahedron Lett.* **33**, 3277 (1992).
- No change was observed in the ¹H NMR spectrum of **1** (1 equivalent) and CHD (5 equivalents) in benzene-*d*₆ (sealed NMR tube) after heating to 95°C for 447.5 hours (CH₂Cl₂ as internal standard).
- Activation energies for some other Bergman cyclizations studied range from 27.4 kcal mol⁻¹ (20) for acyclic enediynes to 19.4 kcal mol⁻¹ (7) for a 10-membered ring. Most relevant is the value of $E_a = 25.1\text{ kcal mol}^{-1}$ determined for the cycloaromatization of 1,2-bis(ethynyl)benzene: J. W. Grissom, T. L. Calkins, H. A. McMillen, Y. Jiang, *J. Org. Chem.* **59**, 5833 (1994).
- This research was supported in part by the Office of Naval Research (to the Massachusetts Institute of Technology) and by the Research Corporation (to Bowdoin College). We thank J. Stubbe and S. L. Schreiber for insightful comments and suggestions.

14 March 1995; accepted 14 June 1995

Confinement-Induced Phase Transitions in Simple Liquids

Jacob Klein and Eugenia Kumacheva

The liquid-to-solid transition of a simple model liquid confined between two surfaces was studied as a function of surface separation. From large surface separations (more than 1000 angstroms) down to a separation corresponding to seven molecular layers, the confined films displayed a liquid-like shear viscosity. When the surface separation was further decreased by a single molecular spacing, the films underwent an abrupt, reversible transition to a solid. At the transition, the rigidity of the confined films (quantified in terms of an "effective viscosity") increased reversibly by at least seven orders of magnitude.

The properties of fluids confined to nanoscopic pores or films differ greatly from the properties of fluids in the bulk. For example, liquid lubricants solidify on being compressed to ultrathin layers (1), gases trapped in nanometer-sized pores order into crystalline arrays (2), and simple liquids confined between solid surfaces undergo layering adjacent to each surface (3, 4). The behavior of such films is of central importance for understanding tribology, adhesion and wear properties (5), the wetting and dewetting of surfaces, and the microfluidity of biological membranes (6); insight into the properties of such films is also important for understanding the rigidity and flow behavior of granular materials (7), ceramics (8), and

advanced composites (9), in which deformation occurs by means of the shearing of thin interfacial layers at grain or phase boundaries. However, at a more fundamental level, the interplay at increasing confinement of the dynamics, thermodynamics, and the molecular structure of the fluids, and their commensurability and interactions with the confining walls, is not yet well understood (10, 11).

Measurements of the dynamic properties of simple liquids suggest that these liquids retain their bulk viscosity for films thicker than approximately 10 molecular diameters (12–14). At the other extreme, highly compressed liquid films confined to one to three molecular layers between smooth solid surfaces display solidlike features, evidenced by a finite yield stress (15–17). Computer simulations and theoretical investigations have

Department of Materials and Interfaces, Weizmann Institute of Science, Rehovot 76100, Israel.

shed much light on the molecular details underlying both structural and dynamic behavior in this highly confined regime (18) and suggest that liquids composed of spherical molecules may undergo a sharp liquid-to-solid transition on confinement to a few monolayers (19). Few experimental studies have addressed the process by which a liquid changes to a solid when confined to a sufficiently small space; it has been reported (10, 20) that a number of liquids, when compressed between parallel plates, undergo a continuous increase in their viscosity as the plate separation decreases below a few nanometers. Here we show how the properties of a simple liquid change from its bulk behavior as it is confined by smooth solid surfaces to progressively thinner films. The confinement induces an abrupt, discontinuous liquid-to-solid transition at a well-defined separation of the surfaces.

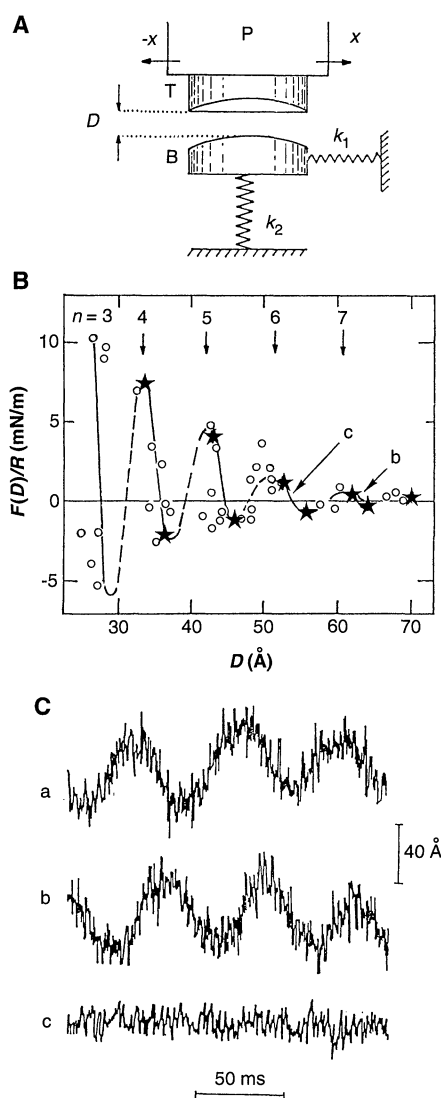
In this report we focus on detailed results for the organic liquid octamethylcyclotetrasiloxane (OMCTS), which, because of its nonpolar nature and the large size of its quasi-spherical molecules (diameter ~ 9 Å), has been used as a model liquid in several earlier investigations (3, 4, 15–17). The surface force balance used in the present study has been described in detail (21) and is shown schematically in Fig. 1A. It has a very

Fig. 1. (A) Schematic of the surface force balance used in this study (21): P is a sectorized piezoelectric tube holding a cylindrical lens T, on which the top mica sheet is mounted. The lower mica sheet is glued onto a second cylindrical lens B, facing and with its cylindrical axis at right angles to the top lens T. The distance of closest approach between the two surfaces in the crossed-cylinder configuration is D . Tube P can provide normal motion (with a spatial resolution of ± 2 Å) to induce changes in the surface separation D ; and it can move the upper surface laterally ($\pm x$ direction) and parallel to the lower surface to within 0.5 Å over the entire range (200 nm) of lateral displacement applied. The springs k_1 and k_2 measure the shear [$F_{\parallel}(D)$] and normal [$F(D)$] forces directly and simultaneously; their bending is monitored to ± 2 Å by an air-gap capacitor bridge and multiple beam interference, respectively. **(B)** Normal force-distance profile $F(D)/R$ between mica sheets immersed in OMCTS (22) [R (≈ 1 cm) is the mean mica surface curvature]. The number n of monolayers corresponding to each force maximum is indicated. Data (at extrema) obtained by Christenson (3) are shown for comparison (stars). Points b ($n = 7$) and c ($n = 6$) refer to the actual positions in the $F(D)/R$ plane where traces b and c, respectively, in the figure were recorded. The temperature throughout the experiments was $23.5^\circ \pm 0.2^\circ\text{C}$. **(C)** The traces are from direct recordings (on a recording oscilloscope) of the time variation of the relative lateral displacement Δx of the mica surfaces (with no applied lateral motion) at separations $D = 1160$ Å (trace a), $D = 62 \pm 2$ Å (trace b), and $D = 54 \pm 2$ Å (trace c); traces b and c correspond, respectively, to points b and c on the force-distance profile in (B).

high sensitivity for the direct measurement of shear forces as well as the normal surface forces acting between two atomically smooth mica surfaces and provides extremely parallel lateral motion between the surfaces even when they are not in contact. These properties of the balance enable us to measure shear forces directly at very low normal stresses without the need for substantial flattening of the mica sheets (with the attendant necessary high compression of the confined films), which has been a feature of earlier shear measurements in simple liquids (15–17).

We first determined the normal force profile $F(D)$ acting between the mica surfaces across OMCTS (22) (Fig. 1B), where D is the surface separation. Oscillations with a periodicity roughly equal to the molecular diameter, as observed in several studies (3, 4), indicate a layering of the OMCTS molecules between the surfaces.

The sharp change in the dynamic properties of the confined liquid with decreasing surface separation is seen qualitatively in the



traces shown in Fig. 1C. These traces record directly the variation with time of the relative lateral motion in the liquid, Δx , between the two mica surfaces. At large surface separations D and with no motion applied to the top surface, Δx responds to external ambient noise at the characteristic frequency (~ 17 Hz) of the spring k_1 (trace a of Fig. 1C) ($D = 1160$ Å). When the surfaces were brought closer together, these random vibrations persisted down to $D = 62 \pm 2$ Å (trace b of Fig. 1C); this corresponds to point b on the normal force profile $F(D)$ (Fig. 1B), at $n = 7$ molecular layers of OMCTS. Upon slight further compression, the surface separation decreased discontinuously to $D = 54 \pm 2$ Å (point c on the normal force profile, Fig. 1B, corresponding to $n = 6$). At this point (trace c of Fig. 1C, the 17-Hz vibrations abruptly ceased. This transition occurred over time scales shorter than we were able to observe (< 0.5 s). The change in confinement from seven to six molecular layers all at once rendered the film solid enough to resist the random lateral shearing motion induced by the external noise. This ability to sustain a shear stress is a fundamental signature of a solid, whereas a liquid by definition cannot sustain such a stress. The transition is reversible, that is, on increasing

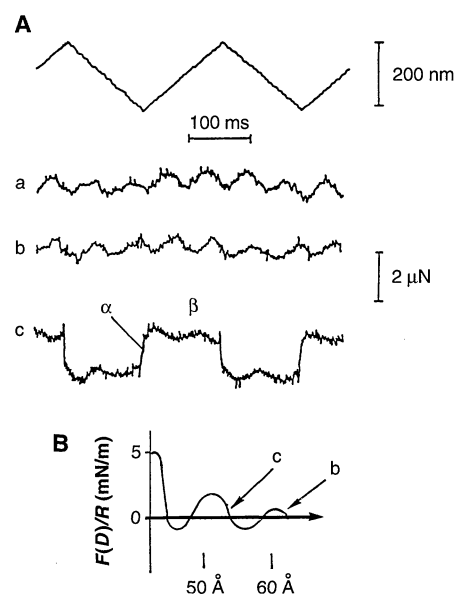


Fig. 2. (A) (Top trace) Lateral back-and-forth motion applied to the top mica surface. (Lower traces) Corresponding measured shear forces for surface separations $D = 1160$ Å (trace a), $D = 62 \pm 2$ Å, $n = 7$ (trace b, point b shown in (B)), and $D = 54 \pm 2$ Å, $n = 6$ (trace c, point c shown in (B)). In trace c, α and β are the elastic and plastic deformation regimes, respectively. Traces represent data averaged over 100 cycles. Most of the residual noise is at the characteristic 17-Hz frequency of spring k_1 . **(B)** The normal force-distance profiles $F(D)/R$ for the separation $D > 40$ Å taken from Fig. 1B, indicating the positions b and c in the $F(D)/R$ plane at which traces b and c in (A) were recorded.

the separation to $D \geq 7$ monolayers, random vibrations (at ~ 17 Hz) were observed once again. Moreover, the transition to the shear stress-sustaining phase is induced by the additional confinement alone: little normal pressure on the OMCTS is necessary. Once the $n = 7 \rightarrow n = 6$ transition has taken place, the confined OMCTS retains its solidlike characteristics even if the applied small normal force (corresponding to point c in Fig. 1B) is reduced to zero.

We obtained a more quantitative measure of this liquid-to-solid transition by applying a controlled lateral motion to the top mica surface by means of the piezoelectric tube and measuring directly the resulting shear force $F_{\parallel}(D)$ between the surfaces. As the top surface is moved laterally at a uniform velocity, first in one direction and then in the other, the shear force transmitted to the lower surface by the confined OMCTS is recorded directly (Fig. 2A). At surface separations from $D = 1160 \text{ \AA}$ down to $D = 62 \pm 2 \text{ \AA}$ ($n = 7$), no shear response was detected within the noise level of the signal (traces a and b of Fig. 2A) [trace b was taken at point b on the $F(D)/R$ (R is the mean

curvature of the mica surfaces) plot in Fig. 2B]. When the surfaces are moved together to $D = 54 \pm 2 \text{ \AA}$ ($n = 6$), the form of the shear stress transmitted by the OMCTS changes sharply [trace c of Fig. 2A, taken at point c on the $F(D)/R$ plot in Fig. 2B]. The response is now characteristic of a solid confined between two surfaces: an initial elastic regime, as the shear stress rises to a yield point (region α in curve c of Fig. 2A), is followed by a "plastic deformation" of the OMCTS in the gap, as for a ductile solid under shear (23, 24). The two confining surfaces then slide past each other at a uniform mean velocity (region β in curve c).

The shear force data of Fig. 2A, trace b, show that the response $F_{\parallel}(D)$ of OMCTS films only seven molecular layers thick is liquidlike and similar to that of much thicker films, as in trace a, and that both are within the signal resolution δF_{\parallel} . This observation may be used to estimate from our data an upper limit on the viscosity of the OMCTS confined between the mica surfaces (25) and shows that, in its liquidlike state at $n = 7$ just before the liquid-to-solid transition, the mean "effective viscosity," η_{eff} of the film is within this upper limit, $\eta_{\text{eff}} < 3 \text{ P}$ (poise).

Figures 1 and 2 demonstrate that the changes in the mechanical properties of the confined OMCTS phase following the liquid-to-solid transition are striking. A measure of the rigidity of this phase may be obtained from its resistance to creep under stress, a process that may be quantified in terms of η_{eff} . The concept of viscosity does not apply to solids, but it is useful for highlighting the changes that take place at this transition. We obtained an estimate of η_{eff} by monitoring the relaxation of the film in its solidlike phase following an applied shear stress, as illustrated in Fig. 3. At this surface

separation ($n = 6$) and pressure, the mica surfaces interact across a contact area $A = (1.2 \pm 0.3) \times 10^{-10} \text{ m}^2$ (26). The configuration is then one of a film of area A and thickness D subjected to a shear force F_{\parallel} applied by means of a spring of constant k_1 (see Fig. 1A for the schematic). Initially, the film confined between the two surfaces is under zero shear force, $F_{\parallel} = 0$ (region a in Fig. 3B); at point b a steady lateral motion at velocity $v_s = (dx/dt)$ is applied to the top surface, equivalent to pulling the end of the spring k_1 at that velocity. At first the spring stretches as the shear force across the film rises (region c) to a yield value $F_{\parallel,y}$. Subsequently, the surfaces slide past each other with a mean velocity v_s : in this regime (region d in Fig. 3B), the mean tension in the spring (and thus the shear force across the film) remains constant at $F_{\parallel} = F_{\parallel,y}$. The applied motion is then stopped (Fig. 3B, point e), and the relaxation of the shear force resulting from creep of the confined phase (region f of Fig. 3B) can be monitored by observing the change in F_{\parallel} . For this configuration, the shear force across a film with mean viscosity η_{eff} decays exponentially with a characteristic time given by $\tau = A \eta_{\text{eff}}/k_1 D$ (Fig. 3A). Thus, for a decay in the force of ΔF_{\parallel} ($\ll F_{\parallel,y}$) over a time Δt , the effective viscosity is given by

$$\eta_{\text{eff}} = \left(\frac{F_{\parallel,y}}{\Delta F_{\parallel}} \right) k_1 D \Delta t A^{-1}$$

As seen from Fig. 3B, the decay ΔF_{\parallel} of the shear force is within the noise level δF_{\parallel} of the signal over a period $\Delta t = 10 \text{ s}$. This imposes a lower limit on η_{eff} given by $(F_{\parallel,y}/\delta F_{\parallel})k_1 D \Delta t A^{-1} \approx 4.10^7 \text{ P}$ (with $k_1 = 300 \text{ N/m}$ and, from Fig. 3B, $F_{\parallel,y} = 9.5 \text{ \mu N}$, and $\delta F_{\parallel} = 0.4 \text{ \mu N}$). The η_{eff} of the OMCTS phase confined to $n = 6$ monolayers must then equal or exceed this lower limit, that is, $\eta_{\text{eff}} \geq 4.10^7 \text{ P}$. The change in η_{eff} of the confined OMCTS film at the transition is illustrated in Fig. 4.

The effective mean viscosity of the confined OMCTS film, which provides a measure of film rigidity, that is, its resistance to creep, increases by at least seven orders of magnitude at the transition, with the limits being set by the signal-to-noise ratio of our measurements. Very similar observations have been made for cyclohexane (27). Within the range of our experimental parameters, we observe no intermediate regime of progressively increasing viscosity on increasing confinement for either of these simple liquids (28). The abruptness, reversibility, and magnitude of the change at the confinement-induced transition indicate a first-order rather than a glass transition and suggest that at the transition, the entire film locks into an ordered, solid structure. Moreover, this transition is brought about by increasing confinement alone, with little ap-

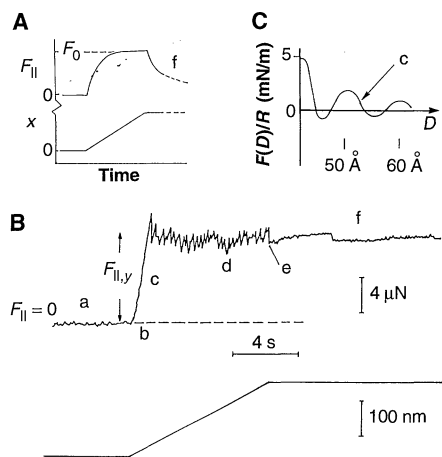


Fig. 3. (A) Schematic variation of the shear force F_{\parallel} expected across a film of area A and effective viscosity η_{eff} confined to a thickness D between the two mica surfaces (Fig. 1A), as the lateral displacement x of the top surface is varied in time. In regime f after the applied lateral motion (dx/dt) is stopped, the force relaxes as $F_{\parallel} = F_0 e^{-t/\tau}$, where $\tau = (A \eta_{\text{eff}}/k_1 D)$ (17); k_1 is the constant of the shear force-measuring spring (Fig. 1A). (B) Applied lateral motion of the upper mica surface (lower trace) and corresponding changes (upper trace) in the shear force $F_{\parallel}(D)$ across the confined OMCTS film, for $D = 54 \pm 2 \text{ \AA}$ ($n = 6$), corresponding to point c in the $F(D)/R$ plane shown in Fig. 2B. In region d, stick-slip motion is clearly seen. The relaxation of the yield force $F_{\parallel,y}$ in region f is within the noise level of the signal over the time shown. (C) The normal force-distance profiles $F(D)/R$ for the separation $D > 40 \text{ \AA}$ (taken from Fig. 1B), indicating position c in the $F(D)/R$ plane at which the trace in (B) was recorded. For this point, the area of the confined film is $A = (1.2 \pm 0.3) \times 10^{-10} \text{ m}^2$ (26).

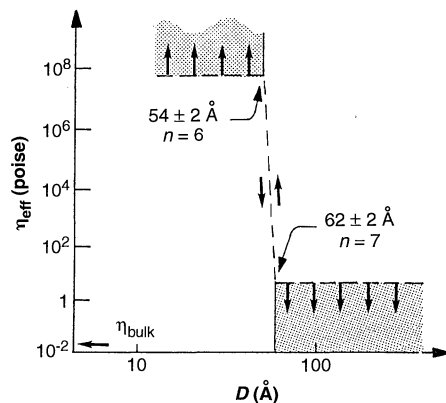


Fig. 4. Variation with film thickness D of the effective mean viscosity η_{eff} of the confined OMCTS film (on a double-logarithmic plot) determined as described in the text. The broken lines at $D < 54 \text{ \AA}$ and at $D > 62 \text{ \AA}$ are lower and upper limits on η_{eff} , respectively. The bulk viscosity of OMCTS at 23°C is indicated.

plied pressure. The fact that this effect is seen for liquids (cyclohexane and OMCTS), whose molecular size differs appreciably from each other as well as from the crystal periodicity of the confining mica surfaces, indicates that epitaxy is not necessary for inducing the transition in such simple liquids.

REFERENCES AND NOTES

1. D. Tabor, *Friction* (Doubleday, New York, 1973).
2. A. Vom Felde et al., *Phys. Rev. Lett.* **53**, 922 (1984); C. Templier et al., *C. R. Acad. Sci.* **299**, 613 (1984); J. H. Evans and D. J. Marzey, *J. Phys. F* **15**, L1 (1985); M. W. Finnis, *Acta Metall.* **35**, 2543 (1987).
3. H. K. Christenson, *J. Chem. Phys.* **78**, 6906 (1983).
4. R. G. Horn and J. N. Israelachvili, *ibid.* **75**, 1400 (1981).
5. F. P. Bowden and D. Tabor, *The Friction and Lubrication of Solids* (Clarendon, Oxford, 1964).
6. F. M. Etzler and W. Drost-Hansen, *Adv. Chem. Ser.* **188**, 486 (1980).
7. H. M. Jaeger and S. R. Nagel, *Science* **255**, 1523 (1992).
8. J. B. Wachtman Jr., Ed., *Tribological Properties of Structural Ceramics* (Academic Press, San Diego, CA, 1989); D. R. Clarke, *Annu. Rev. Mater. Sci.* **17**, 254 (1987), and references therein; J. E. Marion, C. H. Hsueh, A. G. Evans, *J. Am. Ceram. Soc.* **70**, 708 (1987); D. Clarke, *ibid.*, p. 15.
9. L. T. Drzal, *Adv. Polym. Sci.* **75**, 1 (1985).
10. S. Granick, *Science* **253**, 1374 (1991).
11. J. F. Belak, Ed., "Nanotribology" [in *Mater. Res. Soc. Bull.* **18** (no. 5), 15-60 (1993)].
12. D. Y. C. Chan and R. G. Horn, *J. Chem. Phys.* **83**, 5311 (1985); J. N. Israelachvili, *Colloid Polym. Sci.* **264**, 1060 (1986).
13. R. G. Horn, D. T. Smith, W. Haller, *Chem. Phys. Lett.* **162**, 404 (1989).
14. J. Klein et al., *Macromolecules* **26**, 5552 (1993).
15. J. N. Israelachvili, P. M. McGuiggan, A. M. Homola, *Science* **240**, 189 (1988).
16. J. Van Alsten and S. Granick, *Phys. Rev. Lett.* **61**, 2570 (1988).
17. M. L. Gee, P. M. McGuiggan, J. N. Israelachvili, A. M. Homola, *J. Chem. Phys.* **93**, 1895 (1990).
18. See, for example, I. Bitsanis, J. Magda, M. Tirrell, H. T. Davis, *ibid.* **87**, 1733 (1987); U. Landman, W. D. Luedtke, M. W. Ribarsky, *J. Vac. Sci. Technol. A* **7**, 2829 (1989); M. Schoen, C. L. Rhykerd Jr., D. J. Diestler, J. H. Cushman, *Science* **245**, 1223 (1989); P. A. Thompson and M. O. Robbins, *ibid.* **250**, 792 (1990); P. A. Thompson, G. S. Grest, M. O. Robbins, *Phys. Rev. Lett.* **68**, 3448 (1992); D. J. Diestler, M. Schoen, J. H. Cushman, *Science* **262**, 545 (1993).
19. M. Schoen, D. J. Diestler, J. H. Cushman, *J. Chem. Phys.* **87**, 5464 (1987); M. O. Robbins, P. A. Thompson, G. Grest, in (11), p. 45.
20. H. Hsuan-Wei, G. A. Carson, S. Granick, *Phys. Rev. Lett.* **66**, 2758 (1991).
21. J. Klein, D. Perahia, S. Warburg, L. J. Fetters, *Nature* **352**, 143 (1991); J. Klein, E. Kumacheva, D. Mahalu, D. Perahia, L. J. Fetters, *ibid.* **370**, 634 (1994); J. Klein, E. Kumacheva, D. Perahia, D. Mahalu, S. Warburg, *Faraday Spec. Discuss. Chem. Soc.*, in press.
22. OMCTS (purum grade), purchased from Fluka Ltd., was dried for several days over BDH 4A molecular sieve, and then distilled twice over dry nitrogen. The middle fraction distilling at the literature boiling temperature of 175°C was used in the experiments. The liquid was maintained in a dry atmosphere throughout and injected dry into the experimental apparatus, which was also kept dry by a reservoir of P₂O₅.
23. R. W. K. Honeycombe, *The Plastic Deformation of Metals* (Arnold, London, 1984), chap. 6.
24. We find that, as for a ductile solid, the yield stress at a given normal stress is essentially independent of shear velocity.
25. The configuration of the crossed cylindrical mica surfaces near the region of closest approach is that of a sphere, radius $R \approx 1$ cm, a distance D from a plane. The force $F_{\parallel}(D)$ required to move a sphere in a liquid medium of Newtonian viscosity η with velocity v_s

parallel to a plane wall a distance D away, for $D \ll R$, is given by

$$F_{\parallel}(D) = (16\pi/5)v_s\eta R \ln(R/D)$$

[A. J. Goldman, R. G. Cox, H. Brenner, *Chem. Eng. Sci.* **22**, 637 (1967)]. Thus, for $D < 100$ nm, the range of the present study, the force on the moving sphere is dominated by its viscous interactions with the wall. In this regime, it can readily be shown that the effective mean viscosity of the liquid confined to a layer of thickness D is given by

$$\eta_{\text{eff}} \approx \frac{[\partial F_{\parallel}(D)/\partial D]}{2\pi R \dot{\gamma}}$$

where $\dot{\gamma} = (v_s/D)$ is the shear rate at the point of closest approach. In our experiments, $F_{\parallel}(D)$ is within the noise level $|\delta F_{\parallel}(D)| \approx 0.5 \mu\text{N}$ throughout the range $\Delta D = 116$ to 6.2 nm, as seen from curves a and b of Fig. 2A. Putting $\delta F_{\parallel}(D)/\Delta D$ as an upper estimate on $\partial F_{\parallel}(D)/\partial D$ in this range, we find that for $D = 6.2$ nm (that is, seven monolayers of OMCTS) and $v_s = 1600$ nm/s (Fig. 2), this gives an upper estimate on η_{eff} of ~ 3 P.

26. The area A results from the deformation of the mica

surfaces under the known normal and adhesive forces corresponding to point c in Fig. 3C. It is evaluated by means of the Johnson-Kendall-Roberts contact mechanics model [K. L. Johnson, K. Kendall, A. D. Roberts, *Proc. R. Soc. London Ser. A* **324**, 301 (1971)], giving (for point c in Fig. 3C) $A = (1.2 \pm 0.3) \times 10^{-10}$ m².

27. E. Kumacheva and J. Klein, unpublished data.
 28. This is in contrast to earlier reports of such a regime in a number of liquids (including OMCTS) (10, 20). These earlier reports were concerned with thinner films under significant compression, where different effects may play a role. Further work will be required to clarify the relation between the different studies.

29. We thank R. Ball, S. Granick, G. Grest, J. Israelachvili, M. Lahav, L. Leiserovicz, and M. Robbins for useful discussions and comments. This work was supported by the Israel Science Foundation, the Commission of the European Community, and the Ministry of Science and Arts (Israel) together with the Kernforschungszentrum (Jülich, Germany).

24 January 1995; accepted 3 May 1995

Osmium-187 Enrichment in Some Plumes: Evidence for Core-Mantle Interaction?

Richard J. Walker,* John W. Morgan, Mary F. Horan

Calculations with data for asteroidal cores indicate that Earth's outer core may have a rhenium/osmium ratio at least 20 percent greater than that of the chondritic upper mantle, potentially leading to an outer core with an osmium-187/osmium-188 ratio at least 8 percent greater than that of chondrites. Because of the much greater abundance of osmium in the outer core relative to the mantle, even a small addition of metal to a plume ascending from the D' layer would transfer the enriched isotopic signature to the mixture. Sources of certain plume-derived systems seem to have osmium-187/osmium-188 ratios 5 to 20 percent greater than that for chondrites, consistent with the ascent of a plume from the core-mantle boundary.

Rhenium and osmium are highly siderophile and chalcophile elements. The two elements form a long-lived radiogenic isotope system based on the β^- transition of ¹⁸⁷Re to ¹⁸⁷Os, with a decay constant of $\sim 1.64 \times 10^{-11}$ year⁻¹ (1). The mantle sources for some ocean island basalts (OIBs) (2-6) have elevated ¹⁸⁷Os/¹⁸⁸Os ratios compared with both chondrites and the upper mantle sources of mid-ocean ridge basalts (MORBs) (2), signifying a long-term increase in the Re/Os ratio. This long-term Re/Os enrichment is also indicated for the mantle sources of other types of presumably plume-derived rocks (7). This enrichment can be attributed to several processes. Here we consider the possibility that in some instances the enrichment is a reflection of chemical interaction between the outer core and lower mantle and the subsequent derivation of plume materials

from the core-mantle interface.

Plume-derived melts are generally presumed to come from relatively deep mantle, though whether plumes are ultimately derived from the lower mantle or from mantle above the 670-km seismic discontinuity is still debated (8-10). The cause of the long-term enrichment of Re relative to Os in ¹⁸⁷Os-enriched rocks derived from plumes is not yet known. Previous researchers (2, 3, 11) have ascribed the resultant radiogenic Os in these rocks to the ancient incorporation of recycled oceanic crust into their sources. This model for Os evolution in the mantle sources of some plumes is consistent with previous interpretations for certain types of enriched OIB sources, as revealed by Pb, Sr, and Nd isotopes (10, 12). Also, in OIB samples with very low Os concentrations, enriched Os can result from contamination of the basaltic melt with old, radiogenic oceanic crust (4).

The enrichment of ¹⁸⁷Os in some ocean island sources, however, does not always correlate with enrichments or depletions in other isotopic systems, as would be predicted for the recycling of oceanic crust (6, 13).

R. J. Walker, Isotope Geology Laboratory, Department of Geology, University of Maryland, College Park, MD 20742, USA.

J. W. Morgan and M. F. Horan, M.S. 981, U.S. Geological Survey, Reston, VA 22092, USA.

*To whom correspondence should be addressed.